

## HYBRID FUZZY LOGIC CONTROLLER FOR TRI-PORT CONVERTER FED EV'S WITH PV/FC ENERGY UTILIZATION

G GOPI

Assistant Professor, Department of Electrical and Electronics Engineering, Siddhartha Institute of Technology and Sciences, Narapally, Hyderabad, Telangana, India

**ABSTRACT:** This project presents the switched reluctance motor (SRM) with hybrid renewable system. Switched Reluctance Motors (SRM) has a widerange of industrial applications because of theiradvantages over conventional AC/DC Drives. This is due to simple construction, ruggednessand inexpensive manufacturing potential. Variousmethods have used and applied to control SRM speed generally, the PV-fed EV has a similar structure to thehybrid electrical vehicle, whose internal combustion engine(ICE) is replaced by the hybrid system. A hybrid energy system, or hybrid power, usually consists of two or more renewable energy sources used together to provide increased system efficiency as well as greater balance in energy supply.The PV has different characteristics to ICEs, the maximumpower point tracking (MPPT) and solar energy utilization arethe unique factors for the PV-fed EVs.In order to achieve low cost and flexible energy flow modes,a low cost tri-port converter is proposed in this paper tocoordinate the PV panel, SRM and battery. Hybrid renewables applied in Energy storage like battery technologies, superconducting magnetic energy, capacitors, compressed air and pumped storage, seems to be an alternative method that the operator of an electrical power grid can use to adapt energy production to energy consumption, both of which can vary randomly over time. The proposed tri-port technology with hybrid fuzzy logic controller is developed in MATLAB/SIMULINK environment and the results are proven to be successful in producing reduced harmonic distortion and have the capability to make better market for electric vehicle in the nearby future.

**Key Words:** Electric vehicles, photovoltaic's (PV), power flow control, switched reluctance motors (SRMs), tri-port converter, Fuzzy Logic Controller, Hybrid fuzzy logic controller.

### I. INTRODUCTION

Electric vehicles are automobiles, which are powered by electrical engine and electrical energy. An electric vehicle (EV), also referred to as an electric drive vehicle, uses one or more electric motors or traction motors for propulsion [1]. An electric vehicle may be powered through a collector system by electricity from off-

vehicle sources, or may be selfcontained with a battery or generator to convert fuel to electricity [2]. EVs include road and rail vehicles, surface and underwater vessels, electric aircraft and electric spacecraft [4]. EVs first came into existence in the mid-19<sup>th</sup> century, when electricity was among the preferred methods for

motor vehicle propulsion, providing a level of comfort and ease of operation that could not be achieved by the gasoline cars of the time

[5]. Due to the development of electric vehicles is a very important and prospective process. Electric vehicles are powered by an electric motor instead of an internal combustion engine [6-7]. Electric vehicles are 100% eco-friendly and they do not emit any toxic gases like CO<sub>2</sub>, N<sub>2</sub> etc. which causes Global warming. But there are some downsides in the case of electric vehicles. Due to the limitation of current battery technologies, the driving range is very short. This will reduce the wide application of electric vehicles. In earlier, in terms of motor drives, high-performance permanent magnet (PM) machines are widely used [8]. In PM machines there is no field winding and the field is provided by the permanent magnet. Most commonly rare earth materials are used [9]. But they are very costlier. So by the use of PM machines it will also reduce the wide application of electric vehicles. To overcome these issues a photovoltaic panel and a switched reluctance motor can be used for power supply and motor drive [10]. By introducing PV panel on the top of the vehicle, a suitable energy source can be achieved. PV panel has low power density for traction drives; they can be used to charge the batteries. Also the SRM need no rare earth materials. The switched reluctance motor (SRM) is a type of a stepper motor, an electric motor that runs by reluctance torque [11]. Unlike common DC motor types, power is delivered to windings in the stator (case) rather than the rotor. This greatly simplifies mechanical design as power does not have to be delivered to a moving part, but it complicates the electrical design as some sort of switching

system needs to be used to deliver power to the different windings [12-13]. With modern electronic devices, precisely timed switching is

not a problem, and the SRM is a popular design for modern stepper motors [14]. Its main drawback is torque ripple. Hence, it is necessary to design a hybrid fuzzy controller for SRM to get the optimum performance in the presence of the parameters variations and load disturbances. This study proposes a hybrid fuzzy controller where in discrete PI and fuzzy logic control algorithms are combined to get the desired performance of SRM [15]. This controller employs only with the speed error and changes in speed error and produces an equivalent control term. The designed hybrid fuzzy controller improves system performance in transient and steady state. Generally, the PV-fed EV has a similar structure to the hybrid electrical vehicle, whose internal combustion engine (ICE) is replaced by the PV panel. The PV-fed EV system is illustrated in Fig.1. Its key components include an off-board charging station, a PV, batteries and power converters. In order to decrease the energy conversion processes, one approach is to redesign the motor to include some on-board charging functions. For instance, paper designs a 20-kW split-phase PM motor for EV charging, but it suffers from high harmonic contents in the back electromotive force (EMF). Another solution is based on a traditional SRM. Paper achieves on-board charging and power factor correction in a 2.3-kW SRM by employing machine windings as the input filter inductor. The concept of modular structure of driving topology is proposed in paper. Based on intelligent power modules (IPM), a four-phase half bridge converter is employed to achieve driving and

grid-charging. Although modularization supports mass production, the use of half/full bridge topology reduces the system reliability

(e.g. shoot-through issues). Paper develops a simple topology for plug-in hybrid electrical vehicle (HEV) that supports flexible energy flow. But for grid charging, the grid should be connected to the generator rectifier that increases the energy conversion process and decreases the charging efficiency. Nonetheless, an effective topology and control strategy for PV-fed EVs is not yet developed. Because the PV has different characteristics to ICEs, the maximum power point tracking (MPPT) and solar energy utilization are the unique factors for the PV-fed EVs.

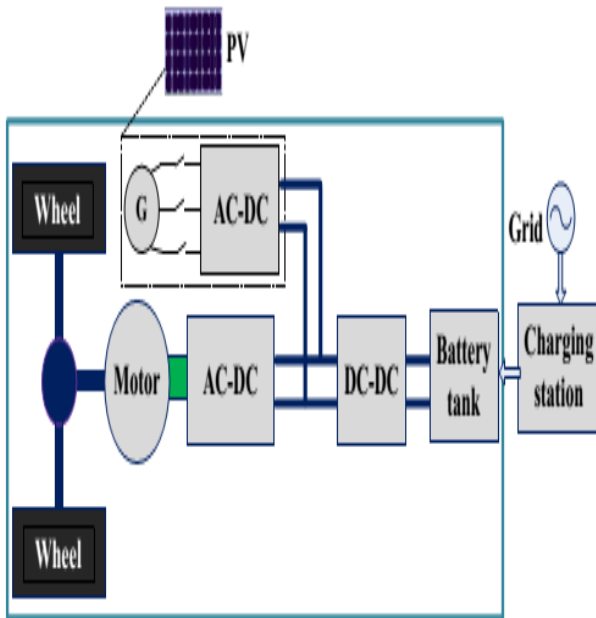


Fig.1 PV-fed hybrid electrical vehicle

## II. TOPOLOGY AND OPERATIONAL MODES

### A. Proposed topology and working modes

The proposed Tri-port topology has three energy terminals, PV, battery and SRM. They are linked by a power converter which consists of four switching devices ( $S_0 \sim S_3$ ), four diodes

( $D_0 \sim D_3$ ) and two relays, as shown in Fig.2. By controlling relays  $J_1$  and  $J_2$ , the six operation modes are supported, as shown in Fig.3; the

corresponding relay actions are illustrated in Table I. In mode 1, PV is the energy source to drive the SRM and to charge the battery. In mode 2, the PV and battery are both the energy sources to drive the SRM. In mode 3, the PV is the source and the battery is idle. In mode 4, the battery is the driving source and the PV is idle. In mode 5, the battery is charged by a single-phase grid while both the PV and SRM are idle. In mode 6, the battery is charged by the PV and the SRM is idle.

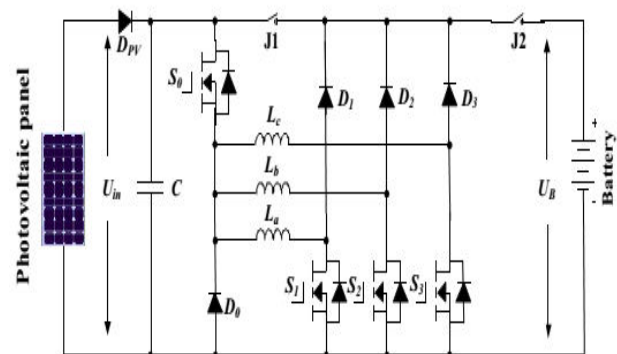


Fig.2. The proposed Tri-port topology for PV-powered SRM drive

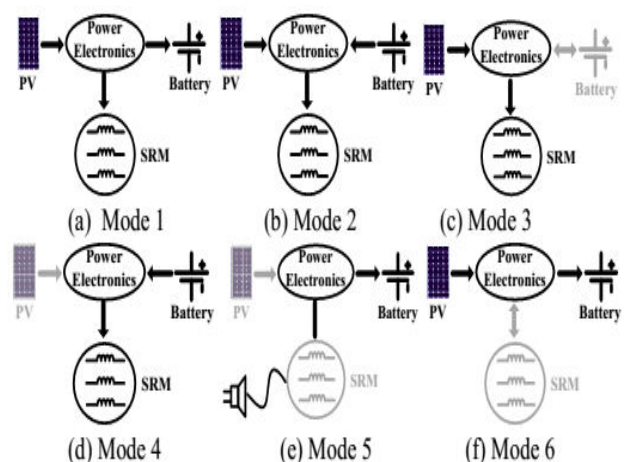


Fig.3. Six operation modes of the proposed Tri-port topology

TABLE 1  $J_1$  and  $J_2$  Actions under Different Modes

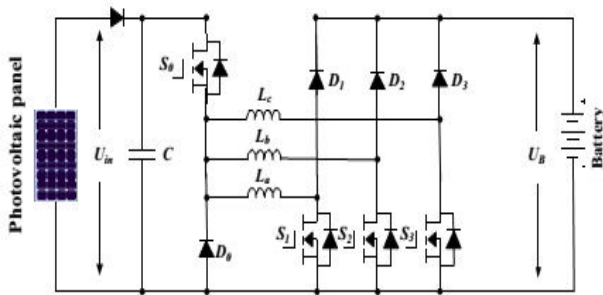
Mode	J1 and J2
1	J1 turn-off; J2 turn-on
2	J1 and J2 turn-on
3	J1 turn-on; J2 turn-off
4	J1 and J2 turn-on
5	J1 and J2 turn-on
6	J1 turn-off; J2 turn-on

## B. Driving modes

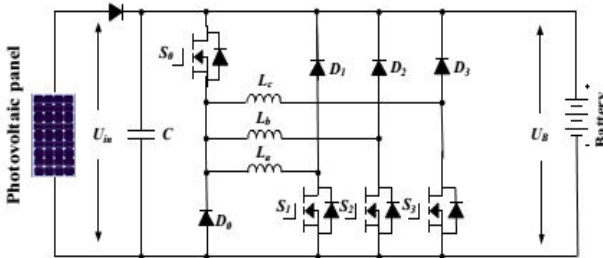
Operating modes 1~4 are the driving modes to provide traction drive to the vehicle.

### (1) Mode 1

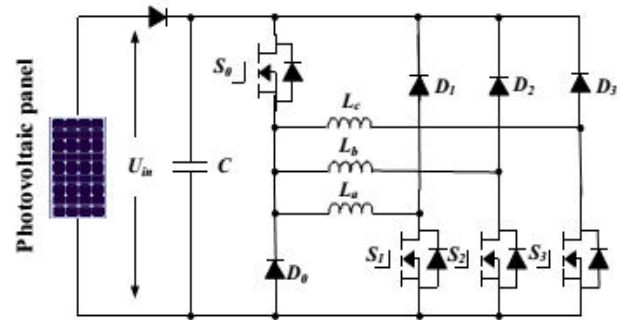
At light loads of operation, the energy generated from the PV is more than the SRM needed; the system operates in mode 1. The corresponding operation circuit is shown in Fig.4 (a), in which relay  $J_1$  turns off and relay  $J_2$  turns on. The PV panel energy feed the energy to SRM and charge the battery; so in this mode, the battery is charged in EV operation condition.



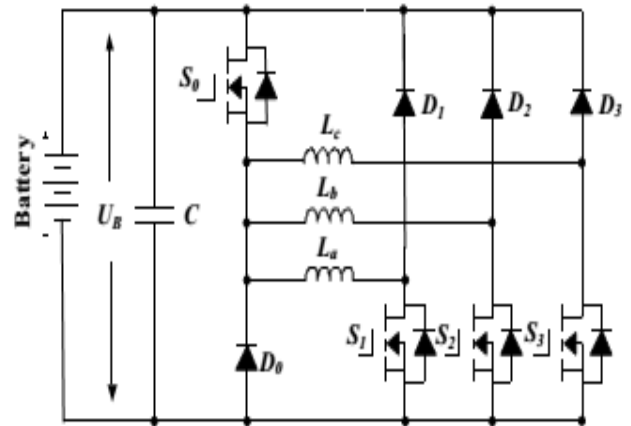
(a) Operation circuit under mode 1



(b) Operation circuit under mode 2



(c) Operation circuit under mode 3



(d) Operation circuit under mode 4

Fig.4 The equivalent circuits under driving modes

### (2) Mode 2

When the SRM operates in heavy load such as uphill driving or acceleration, both the PV panel and battery supply power to the SRM. The corresponding operation circuit is shown in Fig.4(b), in which relay  $J_1$  and  $J_2$  are turned on.

### (3) Mode 3

When the battery is out of power, the PV panel is the only energy source to drive the vehicle. The corresponding circuit is shown in Fig.4(c).  $J_1$  turns on and  $J_2$  turns off.

### (4) Mode 4

When the PV cannot generate electricity due to low solar irradiation, the battery supplies power to the SRM. The corresponding topology is illustrated in Fig.4(d). In this mode, relay  $J_1$  and  $J_2$  are both conducting.

### C. Battery charging modes

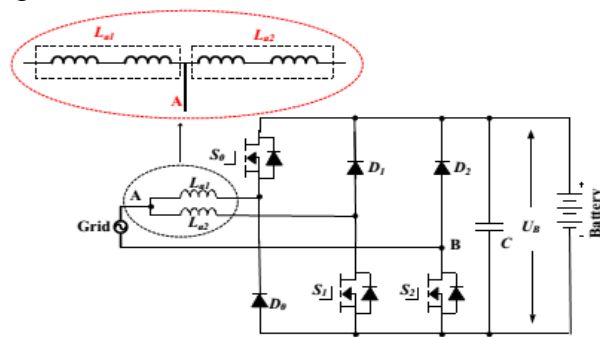
Operating modes 5 and 6 are the battery charging modes.

#### (5) Mode 5

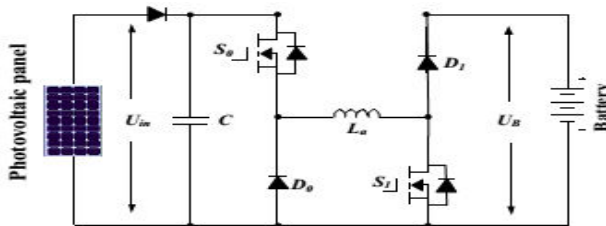
When PV cannot generate electricity, an external power source is needed to charge the battery, such as AC grid. The corresponding circuit is shown in Fig.5(a).  $J_1$  and  $J_2$  turns on. Point A is central tapped of phase windings that can be easily achieved without changing the motor structure. One of the three phase windings is split and its midpoint is pulled out, as shown in Fig.5(a). Phase windings  $L_{a1}$  and  $L_{a2}$  are employed as input filter inductors. These inductors are part of the drive circuit to form an AC-DC rectifier for grid charging.

#### (6) Mode 6

When the EV is parked under the sun, the PV can charge the battery.  $J_1$  turns off;  $J_2$  turns on. The corresponding charging circuit is shown in Fig.5(b).



(a) Grid charging mode



(b) PV source charging mode

Fig.5 Equivalent circuits of charging condition modes

### III. CONTROL STRATEGY UNDER DIFFERENT MODES

In order to make the best use of solar energy for driving the EV, a control strategy under different modes is designed.

#### B. Single source driving mode

According to the difference in the power sources, there are PV-driving; battery-driving and PV and battery parallel fed source. In a heavy load condition, the PV power cannot support the EV, mode 2 can be adopted to support enough energy and make full use of solar energy. Fig.6(a) shows the equivalent power source; the corresponding PV panel working points is illustrated in Fig.6(b). Because the PV is paralleled with the battery, the PV panel voltage is clamped to the battery voltage  $U_B$ . In mode 2, there are three working states: winding excitation, energy recycling and freewheeling states, as shown in Fig.7. Modes 3 and 4 have similar working states to mode 2. The difference is that the PV is the only source in mode 3 while the battery is the only source in mode 4.

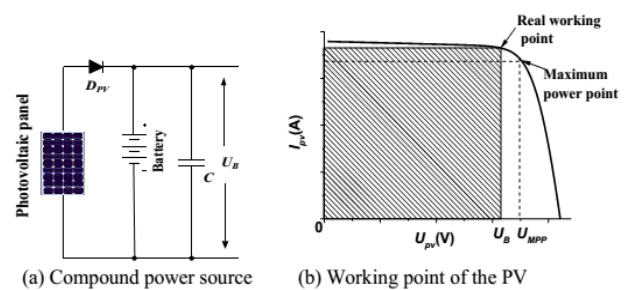
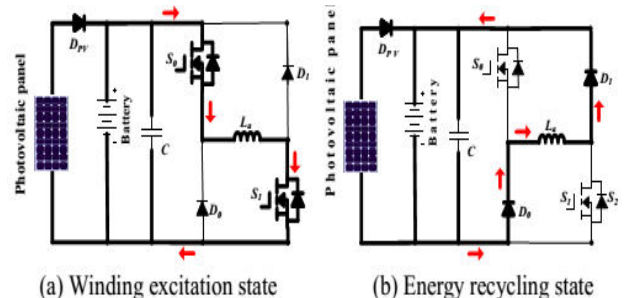
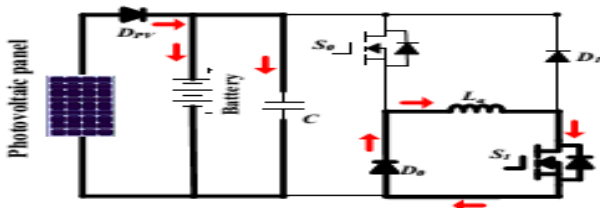


Fig.6 Power supply at mode 2



(a) Winding excitation state

(b) Energy recycling state



(c) Freewheeling state

Fig.7 Working states at mode 2

Neglecting the voltage drop across the power switches and diodes, the phase voltage is given by

$$U_{in} = R_k i_k + \frac{d\psi(i_k, \theta_r)}{dt} = R_k i_k + L_k \frac{di_k}{dt} + i_k \omega_r \frac{dL_k}{d\theta_r}, \quad k = a, b, c \quad (1)$$

where  $U_{in}$  is the DC-link voltage,  $k$  is phase a, b, or c,  $R_k$  is the phase resistance,  $i_k$  is the phase current,  $L_k$  is the phase inductance,  $\theta_r$  is the rotor position,  $\psi(i_k, \theta_r)$  is the phase flux linkage depending on the phase current and rotor position, and  $\omega_r$  is the angular speed. The third term in Eq.1 is the back electromotive force (EMF) voltage given by

$$e_k = i_k \omega_r \frac{dL_k}{d\theta_r} \quad (2)$$

Hence, the phase voltage is found by

$$U_k = R_k i_k + L_k \frac{di_k}{dt} + e_k \quad (3)$$

In the excitation region, turning on  $S_0$  and  $S_1$  will induce a current in phase a winding, as show in Fig.7(a). Phase a winding is subjected to the positive DC bus voltage.

$$+U_{in} = R_k i_k + L_k \frac{di_k}{dt} + e_k \quad (4)$$

When  $S_0$  is off and  $S_1$  is on, the phase current is in a freewheeling state in a zero voltage loop, as shown in Fig.3.7(c), the phase voltage is zero.

$$0 = R_k i_k + L_k \frac{di_k}{dt} + e_k \quad (5)$$

In the demagnetization region,  $S_0$  and  $S_1$  are both turned off, and the phase current will flow back to the power supply, as show in Fig.7(b). In this state, the phase winding is subjected to the negative DC bus voltage, and the phase voltage is

$$-U_{in} = R_k i_k + L_k \frac{di_k}{dt} + e_k \quad (6)$$

In single source driving mode, the voltage-PWM control is employed as the basic scheme, as illustrated in Fig.8. According to the given speed  $\omega^*$ , the voltage-PWM control is activated at speed control.

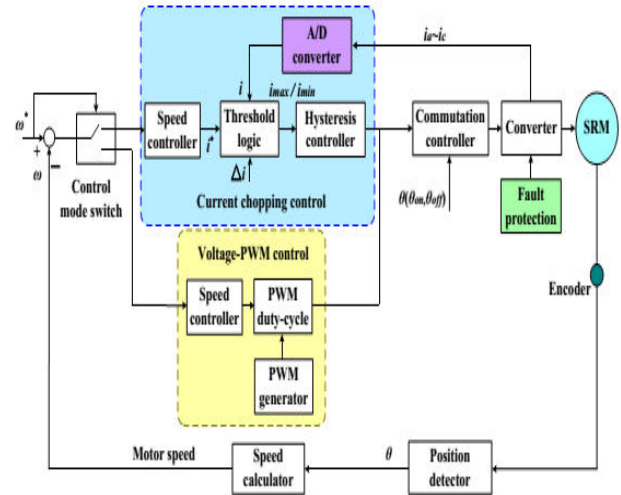


Fig.8 SRM control strategy under single source driving mode

## B. Driving-charging hybrid control strategy

In the driving-charging hybrid control, the PV is the driving source and the battery is charged by the freewheeling current, as illustrated in drive mode 1. There are two control objectives: maximum power point tracking (MPPT) of the PV panel and speed control of the SRM. The dual-source condition is switched from a PV-driving mode. Firstly, the motor speed is controlled at a given speed in mode 3. Then,  $J_2$  is tuned on and  $J_1$  is off to switch to mode 1. By controlling the turn-off angle, the maximum

power of PV panel can be tracked. There are three steady working states for the dual-source mode (mode 1), as shown in Fig.9. In Fig.9(a),  $S_0$  and  $S_1$  conduct, the PV panel charges the SRM winding to drive the motor; In Fig.9(b),  $S_0$  and  $S_1$  turn off; and the battery is charged with freewheeling current of the phase winding. Fig.9(c) shows a freewheeling state.

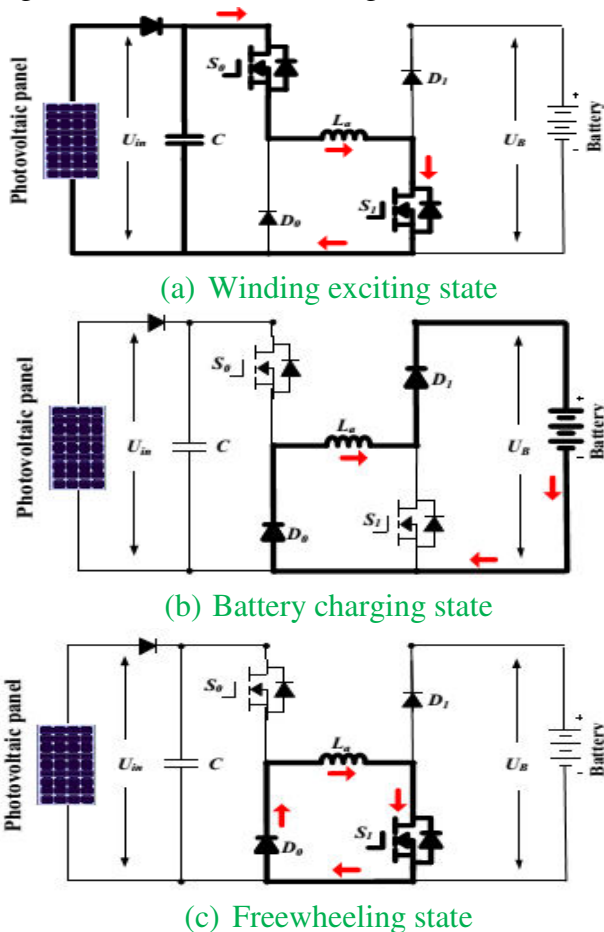


Fig.9 Mode 1 working states

Fig.10 is the control strategy under driving-charging mode. In Fig.10,  $\theta_{on}$  is the turn on angle of SRM;  $\theta_{off}$  is the turn-off angle of SRM. By adjusting turn-on angle, the speed of SRM can be controlled; the maximum power point tracking of PV panel can be achieved by adjusting turn-off angle, which can control the charging current to the battery.

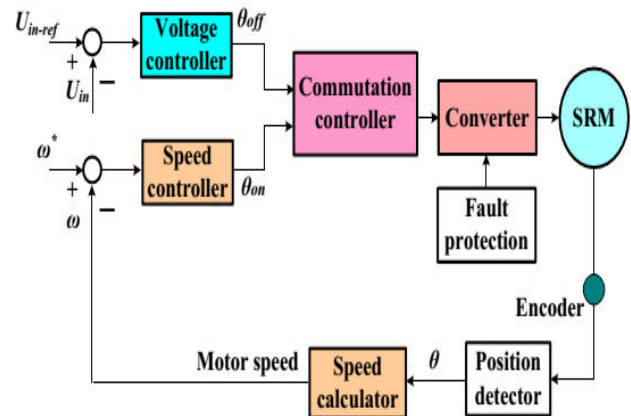


Fig.10. Control strategy under driving-charging mode (mode 1)

### C. Grid-charging control strategy

The proposed topology also supports the single-phase grid charging. There are four basic charging states and  $S_0$  is always turned off. When the grid instantaneous voltage is over zero, the two working states are presented in Fig.11(a) and (b). In Fig.11(a),  $S_1$  and  $S_2$  conduct, the grid voltage charges the phase winding  $L_{a2}$ , the corresponding equation can be expressed as Eq.7; In Fig.11(b),  $S_1$  turns off and  $S_2$  conducts, the grid is connected in series with phase winding to charges the battery, the corresponding equation can be expressed as Eq.8.

$$U_{grid} = L_{a2} \cdot \frac{di_{grid}}{dt} \quad (7)$$

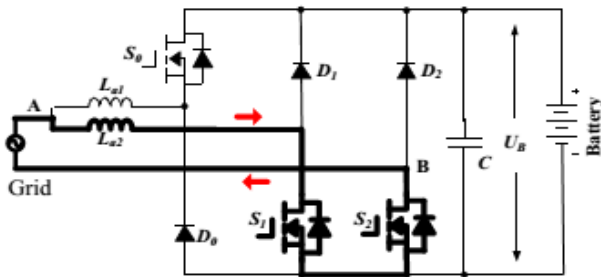
$$U_B - U_{grid} = L_{a2} \cdot \frac{di_{grid}}{dt} \quad (8)$$

When the grid instantaneous voltage is below zero, the two working states are presented in Fig.11 (c) and (d). In Fig.11(c),  $S_1$  and  $S_2$  conduct, the grid voltage charges the phase winding  $L_{a1}$  and  $L_{a2}$ , the corresponding equation can be expressed as Eq. (9); In Fig.11(d),  $S_1$  keeps conducting and  $S_2$  turns off, the grid is

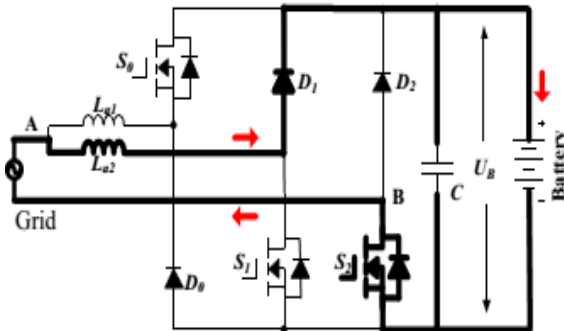
connected in series with phase winding  $L_{a1}$  and  $L_{a2}$  to charges the battery, the corresponding equation can be expressed as Eq.10.

$$U_{grid} = \frac{L_{a1} + L_{a2}}{L_{a1} \cdot L_{a2}} \cdot \frac{di_{grid}}{dt} \quad (9)$$

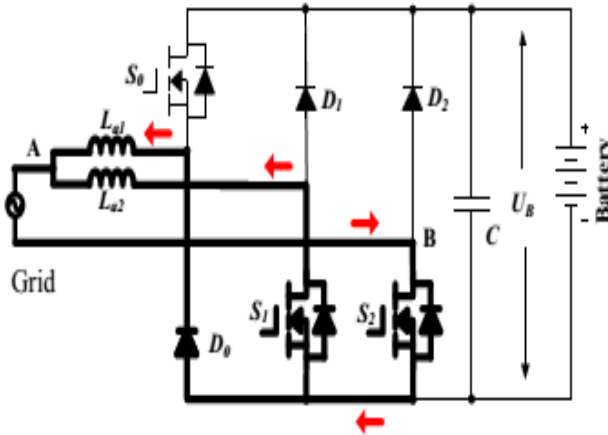
$$-U_B - U_{grid} = \frac{L_{a1} + L_{a2}}{L_{a1} \cdot L_{a2}} \cdot \frac{di_{grid}}{dt} \quad (10)$$



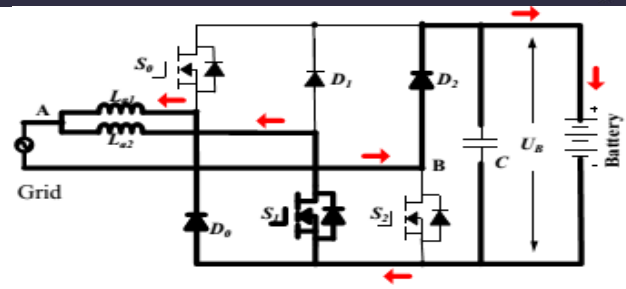
(a) Grid charging state 1 ( $U_{grid} > 0$ )



(b) Grid charging state 2 ( $U_{grid} > 0$ )



(c) Grid charging state 3 ( $U_{grid} < 0$ )



(d) Grid charging state 4 ( $U_{grid} < 0$ )

Fig.11 Mode 5 charging states

In Fig.12,  $U_{grid}$  is the grid voltage; by the phase lock loop (PLL), the phase information can be got;  $I_{ref\_grid}$  is the given amplitude of the grid current. Combining  $\sin\theta$  and  $I_{ref\_grid}$ , the instantaneous grid current reference  $i_{ref\_grid}$  can be calculated. In this mode, when  $U_{grid} > 0$ , the inductance is  $L_{a2}$ ; when  $U_{grid} < 0$ , the inductance is paralleled  $L_{a1}$  and  $L_{a2}$ ; in order to adopt the change in the inductance, hysteresis control is employed to realize grid current regulation. Furthermore, hysteresis control has excellent loop performance, global stability and small phase lag that makes grid connected control stable.

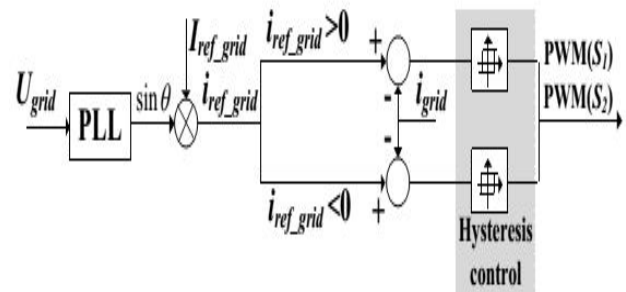


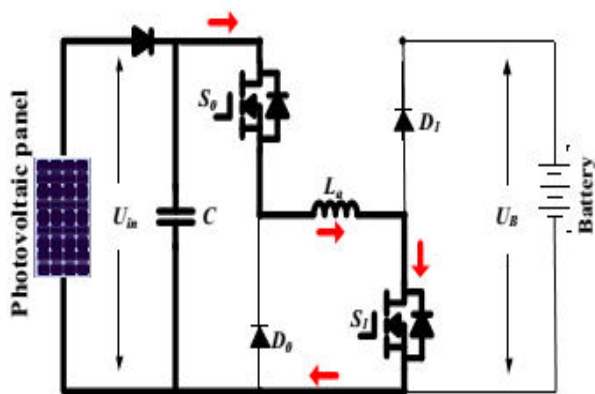
Fig.12 Grid-connected charging control (Mode 5)

### D. PV-fed charging control strategy

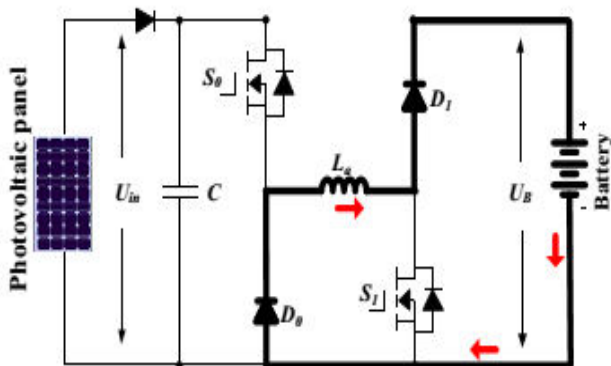
In this mode, the PV panel charges the battery directly by the driving topology. The phase windings are employed as inductor; and the driving topology can be functioned as interleaved Buck boost charging topology. For one phase, there are two states, as shown in



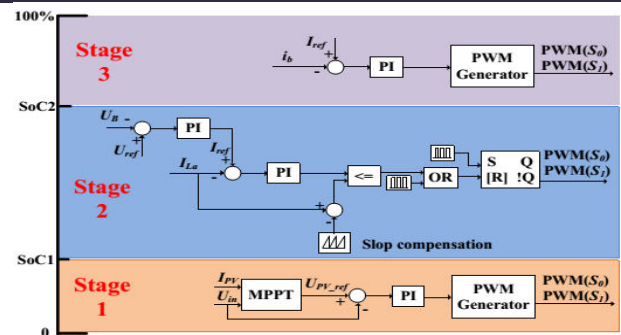
Fig.13(a) and (b). When  $S_0$  and  $S_1$  turn on, the PV panel charges phase inductance; when  $S_0$  and  $S_1$  turns off, the phase inductance discharges energy to battery. According to the state-of-charging (SoC), there are three stages to make full use of solar energy and maintain battery healthy condition, as illustrated in Fig.13 (c). During stage 1, the corresponding battery SoC is in 0~SoC1, the battery is in extremely lack energy condition, the MPPT control strategy is employed to make full use of solar energy. During stage 2, the corresponding battery SoC is in SoC1~ SoC2, the constant voltage control is adapted to charging the battery. During stage 3, the corresponding battery SoC is in SoC2~1, the micro current charging is adapted. In order to simplify the control strategy, constant voltage is employed in PV panel MPPT control.



(a) Phase inductance charging



(b) Battery charging



(c) Charging control strategy.

Fig.13 Mode 6 charging states and control strategy.

## IV. HYBRID FUZZY CONTROLLER

The objective of the hybrid controller is to utilize the best attributes of the PI and fuzzy logic controllers to provide a controller which will produce better response than either the PI or the fuzzy controller. There are two major differences between the tracking ability of the conventional PI controller and the fuzzy logic controller. Both the PI and fuzzy controller produce reasonably good tracking for steady-state or slowly varying operating conditions. However, when there is a step change in any of the operating conditions, such as may occur in the set point or load, the PI controller tends to exhibit some overshoot or oscillations. The fuzzy controller reduces both the overshoot and extent of oscillations under the same operating conditions. Although the fuzzy controller has a slower response by itself, it reduces both the overshoot and extent of oscillations under the same operating conditions. The desire is that, by combining the two controllers, one can get the quick response of the PI controller while eliminating the overshoot possibly associated with it. Switching Control Strategy the switching between the two controllers needs a reliable basis for determining which controller would be more effective.

The answer could be derived by looking at the advantages of each controller. Both controllers yield good responses to steady-state or slowly changing conditions. To take advantage of the rapid response of the PI controller, one needs to keep the system responding under the PI controller for a majority of the time, and use the fuzzy controller only when the system behavior is oscillatory or tends to overshoot. Thus, after designing the best stand-alone PI and fuzzy controllers, one needs to develop a mechanism for switching from the PI to the fuzzy controllers, based on the following two conditions:

- Switch when oscillations are detected;
- Switch when overshoot is detected.

The switching strategy is then simply based on the following conditions: IF the system has an oscillatory behavior then fuzzy controller is activated, Otherwise PI controller is operated. IF the system has an overshoot then fuzzy controller is activated, Otherwise PI controller is operated. The system under study is considered as having an overshoot when the error is zero and the rate of change in error is any other value than zero. The system is considered oscillatory when the sum of the absolute values of the error taken over time does not equal the absolute values of the sum of the error over the same period of time. Since the system is expected to overshoot during oscillatory behavior, the only switching criterion that needs to be considered is overshoot. However, in practice, it is more convenient to directly implement the control signal according to the control actions delivered by the controller. Consequently, the fuzzy controller can be designed so that normal behavior (no oscillations or overshoot) results

in a null fuzzy action as shown in Fig.4. Accordingly, the switching between the two controllers reduces to using PI if the fuzzy has null value; otherwise, the fuzzy output is used. In particular, the fuzzy controller can be designed so that a normal behavior.

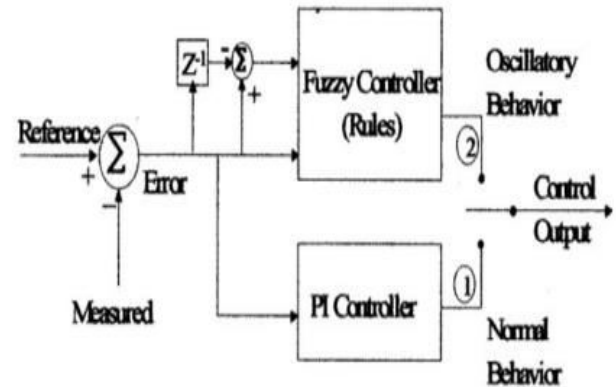


Fig.14 Structure of switching strategy results in a null fuzzy action.

## V. MATLAB/SIMULATION RESULTS

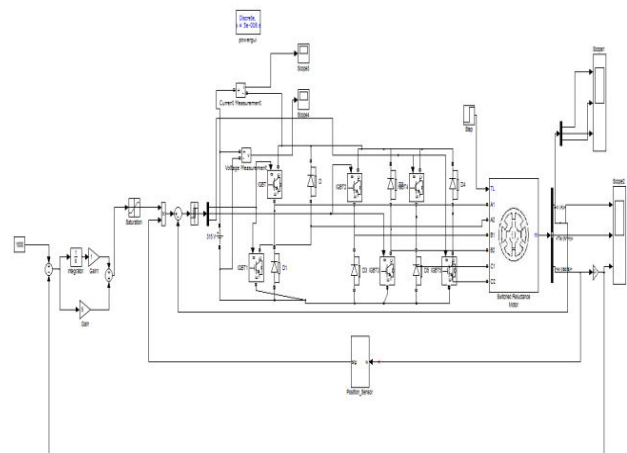
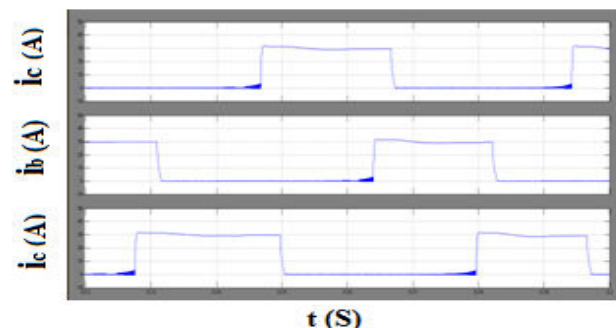
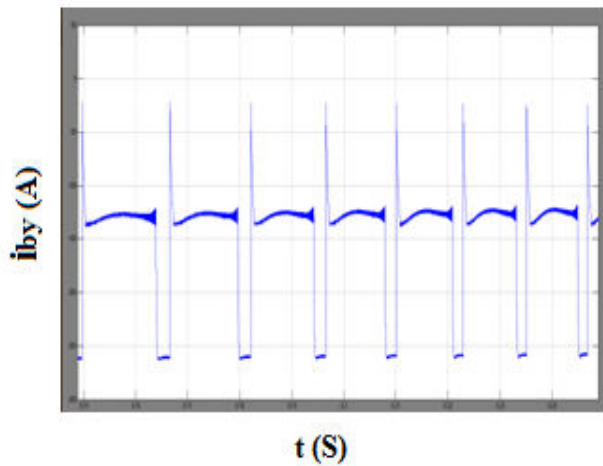
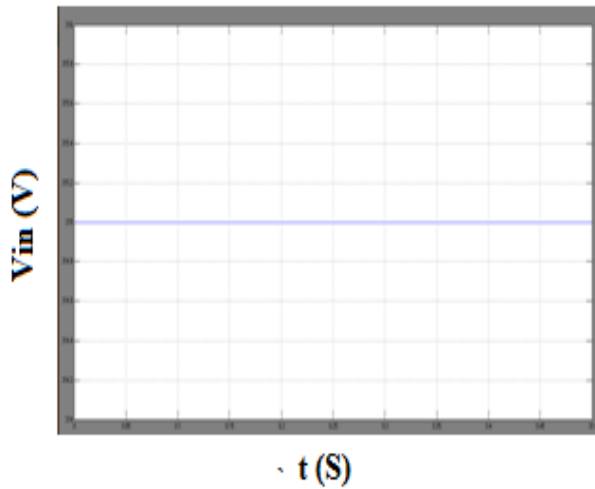
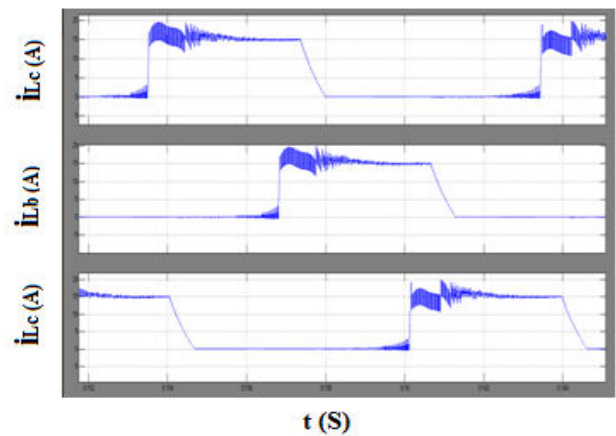
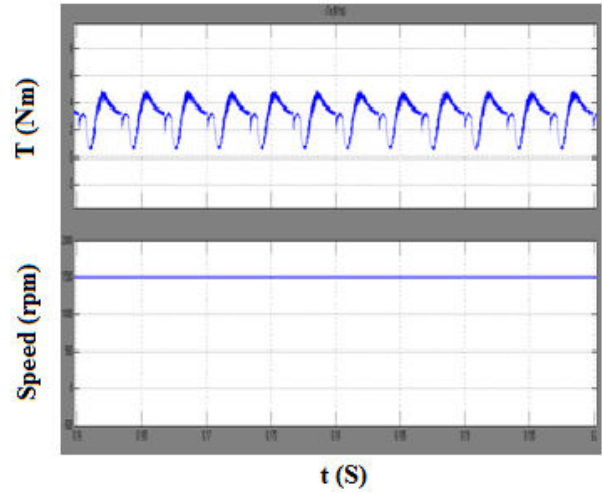


Fig.15 SRM drive model diagram





(a) Simulation results of driving-charging mode (mode 1)



(b) Simulation results of single source driving mode (modes 3 and 4)

Fig.17 Simulation results for driving conditions at modes 1, 3 and 4.

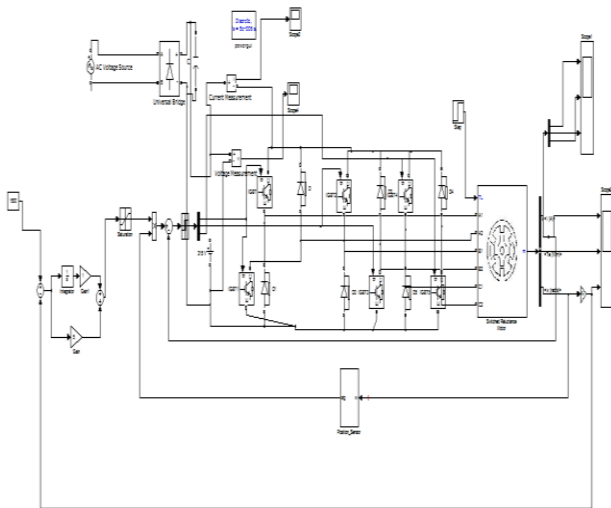


Fig.16 SRM drive model diagram

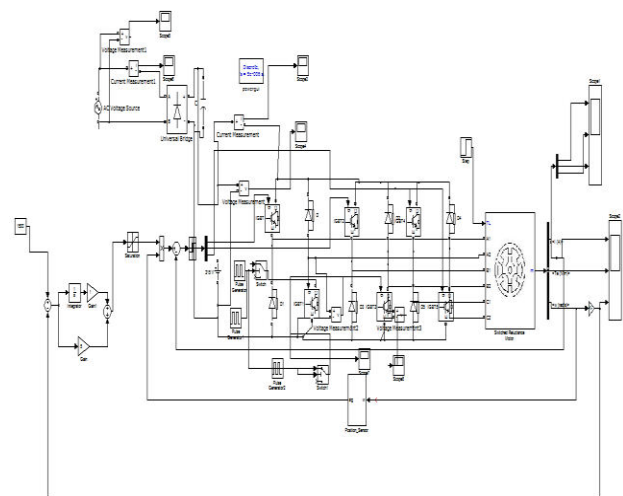
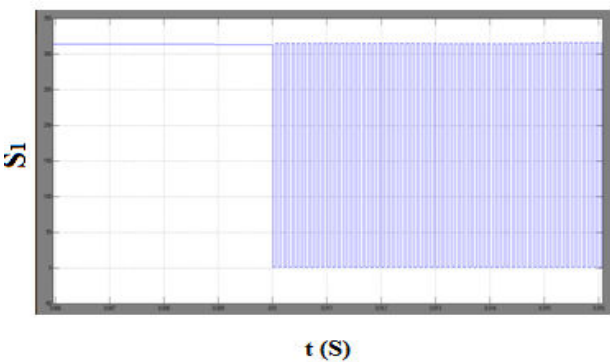
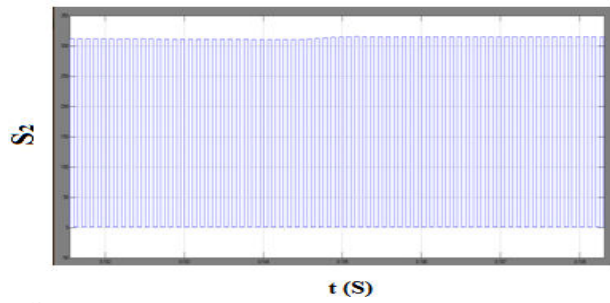
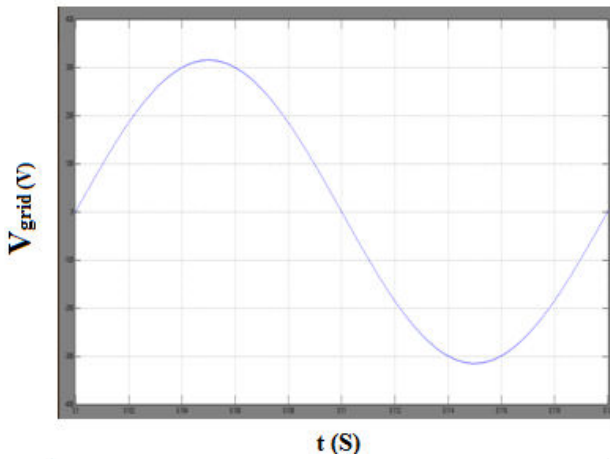
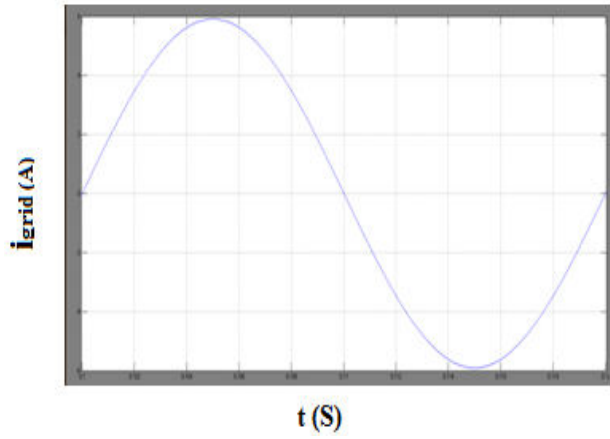


Fig.18 SRM drive model diagram



(a) Grid charging (mode 5)

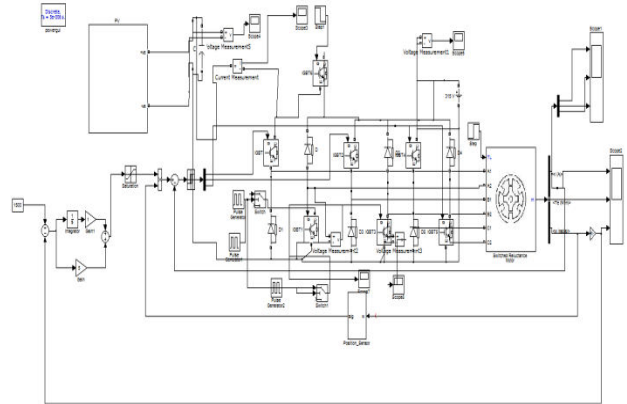
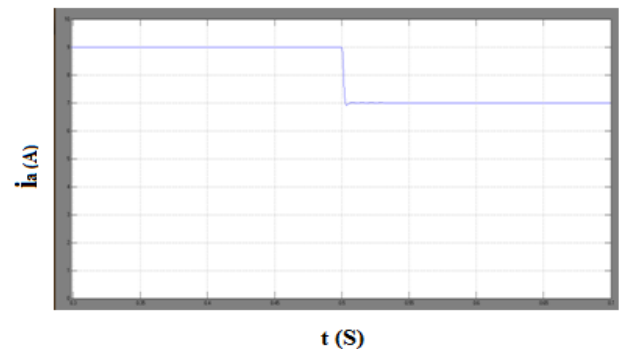
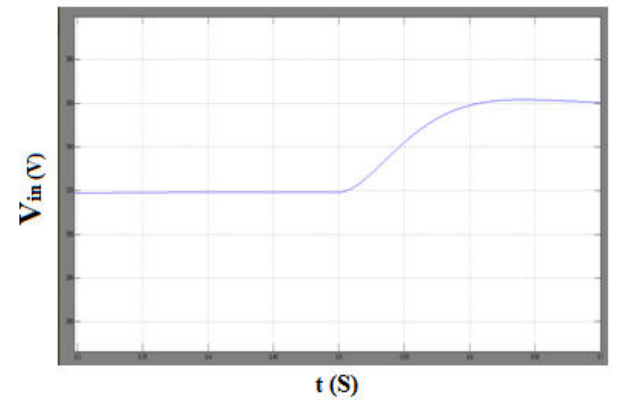
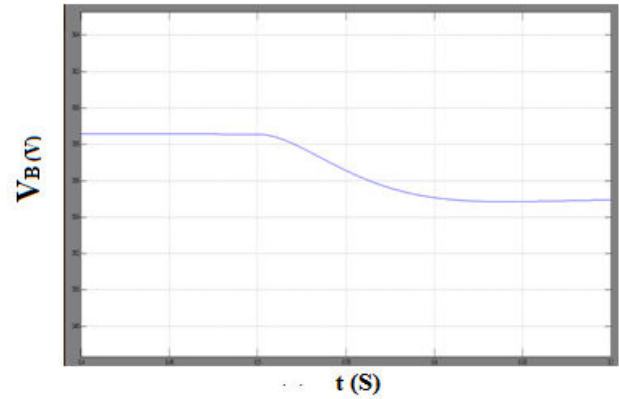


Fig.19 PV-powered SRM drive model diagram



(b) PV charging mode 6 (stage 1 to stage 2)

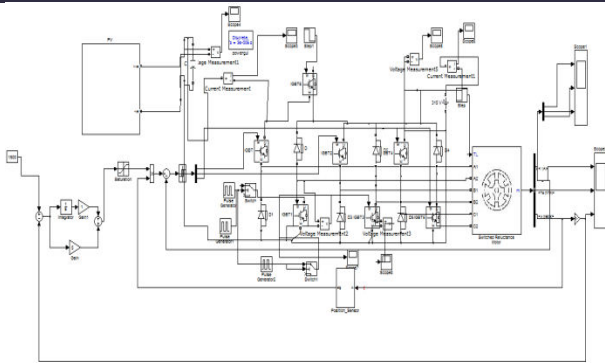


Fig.20 PV-powered SRM drive model diagram

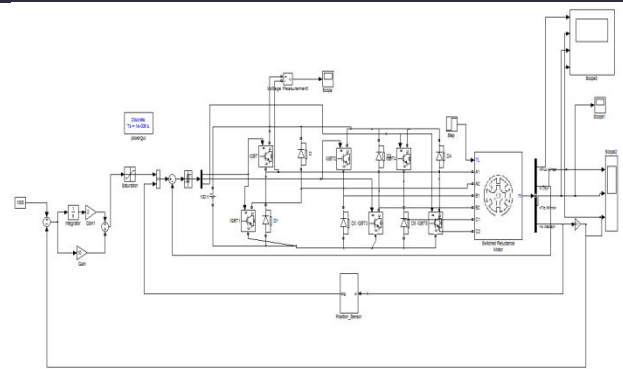
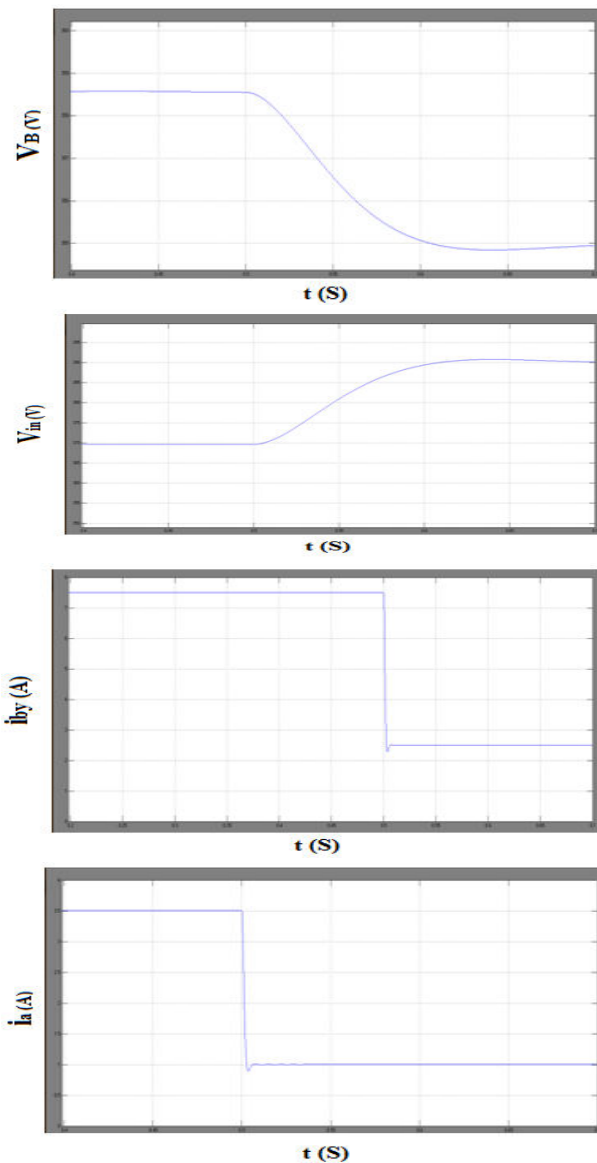


Fig.22 SRM drive model diagram With PI controller



(c) PV charging mode 6 (stage 2 to stage 3)  
Fig.21 simulation results for charging modes.

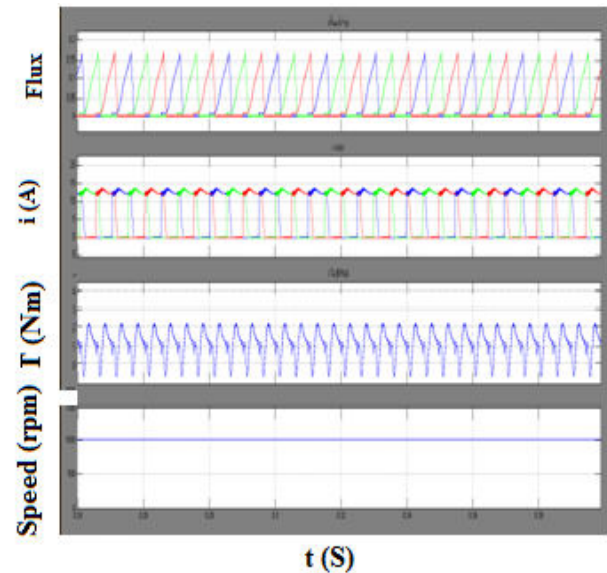


Fig.23 Flux, Current, Speed and Torque

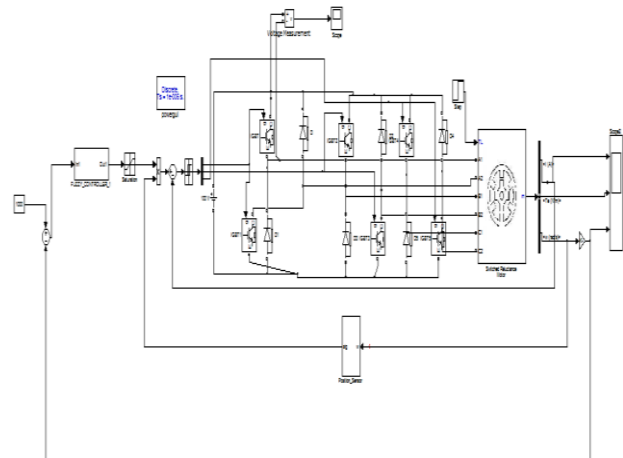


Fig.24 SRM drive model diagram With Fuzzy controller

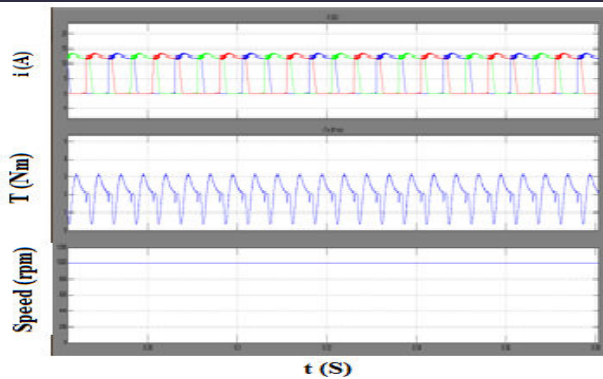


Fig.25 Current, Speed and Torque

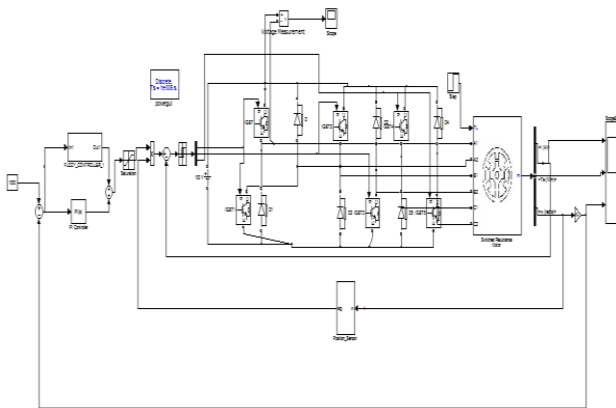


Fig.26 SRM drive model diagram With Hybrid Fuzzy controller

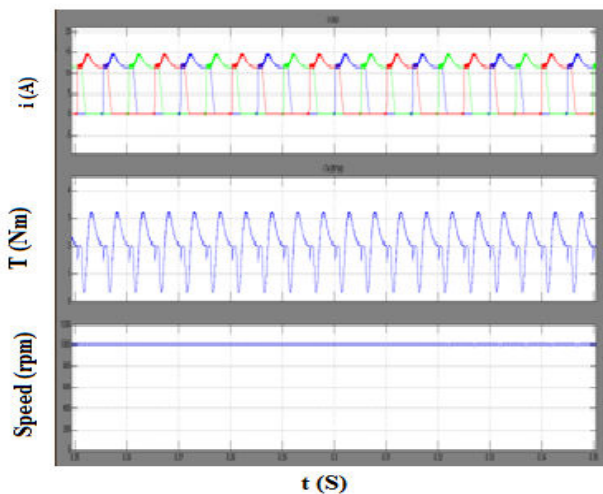


Fig.27 Current, Torque and Speed

## VI. CONCLUSION

In this project in order to tackle the range anxiety of using EVs and decrease the system cost, a combination of the PV panel and SRM is

proposed as the EV driving system. In this a triport converter is used to coordinate the PV panel, battery and SRM. Six working modes are developed to achieve flexible energy flow for driving control, driving/charging hybrid control and charging control. A novel grid-charging topology is formed without a need for external power electronics devices. A PV-fed battery charging control scheme is developed to improve the solar energy utilization. Since PV-fed EVs are a greener and more sustainable technology than conventional ICE vehicles, this work will provide a feasible solution to reducing the total costs and CO<sub>2</sub> emissions of electrified vehicles. It is shown that the presented hybrid controller for SRM drive has fast tracking capability, less steady state error and is robust to load disturbance. The complete speed control scheme of the SRM drive incorporating the hybrid control was implemented. From the above results it is clearly observed that the proposed controller despite of its simple structure has good speed response, high precision speed controller (Hybrid fuzzy) for operating in the whole of speed range and for any loading and environmental conditions were achieved.

## REFERENCES

- [1] Yihua Hu, Chun Gan, and Wenping Cao, "Solar PV powered SRM drive for Evs with flexible energy control functions," IEEE Trans. Ind. Electron., vol. 52, no. 4, pp. 1063–1070, July/Aug.2016.
- [2] A. Emadi, L. Young-Joo, and K. Rajashekara, "Power electronics and motor drives in electric, hybrid electric, and plug-in hybrid electric vehicles," IEEE Trans. Ind. Electron., vol. 55, no. 6, pp. 2237–2245, Jun.2008.

- [3] A. Kuperman, U. Levy, J. Goren, A. Zafransky, and A. Savernin, "Battery charger for electric vehicle traction battery switch station," *IEEE Trans. Ind. Electron.*, vol. 60, no. 12, pp. 5391–5399, Dec. 2013.
- [4] Y. Hu, C. Gan, W. Cao, W. Li, and S. Finney, "Central-tapped node linked modular fault tolerance topology for SRM based EV/HEV applications," *IEEE Trans. Power Electron.*, vol. 31, no. 2, pp. 1541–1554, Feb. 2016.
- [5] Y. Hu, X. Song, W. Cao, and B. Ji, "New SR drive with integrated charging capacity for plug-in hybrid electric vehicles (PHEVs)," *IEEE Trans. Ind. Electron.*, vol. 61, no. 10, pp. 5722–5731, Oct. 2014.
- [6] S. G. Li, S. M. Sharkh, F. C. Walsh, and C. N. Zhang, "Energy and battery management of a plug-in series hybrid electric vehicle using fuzzy logic," *IEEE Trans. Veh. Technol.*, vol. 60, no. 8, pp. 3571–3585, Oct. 2011.
- [7] H. Kim, M. Y. Kim, and G. W. Moon, "A modularized charge equalizer using battery monitoring IC for series-connected Li-ion battery strings in electric vehicles," *IEEE Trans. Power Electron.*, vol. 28, no. 8, pp. 3779–3787, May 2013.
- [8] Ping, Z. Jing, L. Ranran, T. Chengde, and W. Qian, "Magnetic characteristics investigation of an axial–axial flux compound-structure PMSM used for HEVs," *IEEE Trans. Magn.*, vol. 46, no. 6, pp. 2191–2194, Jun. 2010.
- [9] A. Kolli, O. Béthoux, A. De Bernardinis, E. Labouré, and G. Coquery, "Space-vector PWM control synthesis for an H-bridge drive in electric vehicles," *IEEE Trans. Veh. Technol.*, vol. 62, no. 6, pp. 2441–2452, Jul. 2013.
- [10] Y. Hu, C. Gan, W. Cao, W. Li, and S. Finney, "Central-tapped node linked modular fault tolerance topology for SRM based EV/HEV applications," *IEEE Trans. Power Electron.*, vol. 31, no. 2, pp. 1541–1554, Feb. 2016.
- [11] S. M. Yang and J. Y. Chen, "Controlled dynamic braking for switched reluctance motor drives with a rectifier front end," *IEEE Trans. Ind. Electron.*, vol. 60, no. 11, pp. 4913–4919, Nov. 2013.
- [12] B. Bilgin, A. Emadi, and M. Krishnamurthy, "Comprehensive evaluation of the dynamic performance of a 6/10 SRM for traction application in PHEVs," *IEEE Trans. Ind. Electron.*, vol. 60, no. 7, pp. 2564–2575, Jul. 2013.
- [13] M. Takeno, A. Chiba, N. Hoshi, S. Ogasawara, M. Takemoto, and M. Rahman, "Test results and torque improvement of the 50-kW switched reluctance motor designed for hybrid electric vehicles," *IEEE Trans. Ind. Appl.*, vol. 48, no. 4, pp. 1327–1334, Jul./Aug. 2012.
- [14] A. Chiba, M. Takeno, N. Hoshi, M. Takemoto, S. Ogasawara, and M. A. Rahman, "Consideration of number of series turns in switched reluctance traction motor competitive to HEV IPMSM," *IEEE Trans. Ind. Appl.*, vol. 48, no. 6, pp. 2333–2340, Nov./Dec. 2012.
- [15] I. Boldea, L. N. Tutelea, L. Parsa, and D. Dorrell, "Automotive electric propulsion systems with reduced or no permanent magnets: An overview," *IEEE Trans. Ind. Electron.*, vol. 60, no. 9, pp. 5696–5710, Oct. 2014.